Closed-form solution for peak crushing force of the S-rails

A.Khalkhali [1, *], V. Agha Hosseinali Shirazi[2], M. Mohseni Kabir[3]

1 Assistant professor, 2 BSc Student, 3 BSc Student, School of automotive engineering, Iran University of science and technology

* Corresponding Author

Abstract

One of the most important structural components of engine compartment assembly in a car body is the S-rail. S-rails has significant role in absorbing energy during crash events and therefore it is designed for efficient behavior in such conditions. Driving the peak crushing force of the S-rails is one of the important objectives in the design process of such structures. Peak crushing force is exactly the force applied to the downstream components and then will be transferred to the cabin of vehicle. In this paper, closed form solution is performed to drive the peak crushing force of the S-rails. Results of such analytical model finally are compared with the results of finite element simulation. Good agreement between such results shows the accuracy of the proposed analytical model.

Keywords: *S-rail, Peak crushing force, Closed-form solution, Finite element simulation.*

1. Introduction

Structural components of the front of the car body to avoid interference with other components are usually curved. One of the most important structural components of front of the car engine compartment which absorb most of car accident energy is the S-rail. Crushing behavior of the s-rail has been studied experimentally, numerically and analytically by some previous works. Ni [1] represented the impact response of curved box beam using both numerical methods and empirical formulas. Kim and Wierzbicki [2] addressed the design aspect of a front side rail structure of an automobile body concerning weight efficiency and crush energy absorption. They investigated various method of internal strengthening in order to improve structural crashworthiness and performance. Kim and Wierzbicki [3] derived the analytical solution of crushing resistance of thin-walled S-shape frames with rectangular cross-section and compared the results with those of numerical simulation. Zheng and Wierzbicki [4] represented a combined experimental, analytical and numerical study on the quasi static axial crushing of thin-walled aluminum S-rail with circular cross-section. Hosseini-Tehrani [5] showed that a hybrid S-frame made of steel and alumimium gives better characteristic regarding passenger safety and weight efficiency.

Simplified model of the s-rail is depicted in Figure1. According to this figure any variation of geometric parameters which are denoted as radius of curvature (R), curve angle (θ), web width (W), wall thickness (t), and offset of two-end par (D) will lead to new design and new behavior. It should be noted that both the straight lengths (l1 and l3) and oblique length (l2) are derived variables, depending on the values of the curve angle and curve radius.

In this paper, theoretical analysis is performed to obtain peak crushing force of the s-rail with respect to geometrical design parameters. In this way Castiglione's strain energy theory is used to determine cross sectional bending loads along the s-rail. Secondly, effects of section geometry on location of the neutral axis are studied. Quasi static simulation of the s-rail is then performed using commercial software ABAQUS/Explicit. Finally results of numerical and theoretical analysis are compared. Such comparisons show good accuracy of the analytical approach presented in this paper.

2. General formulation

The load and boundary conditions applied on the S-rail are considered according to the Figure 2. Free-body diagram of the S-rail under the applied load P in accordance to the Figure 2 is depicted in Figure 3 where Qf, Pf and Qa are the reaction forces and Ma and Mf are the reaction moments

Created with nitroPDF professional
download the free trial online at nitropdf.com/professional

Downloaded from www.iust.ac.ir at 20:04 IRST on Friday March 3rd 2017

[Downloaded from ijae.iust.ac.ir on 2026-09-12]

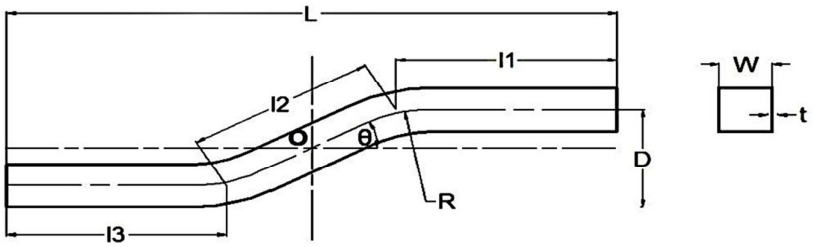

Fig1. Geometrical design parameters of the idealized S-rail

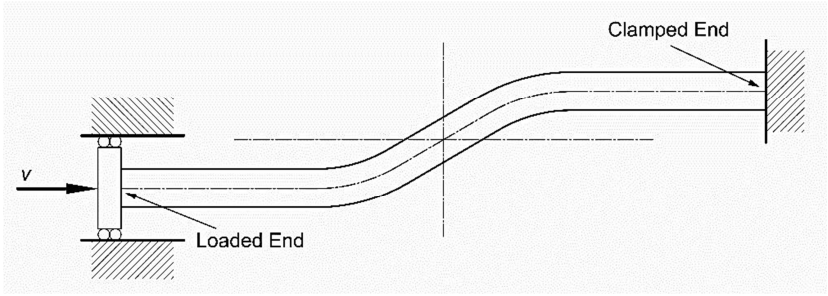

Fig2. Load and boundary conditions considered in the mathematical model

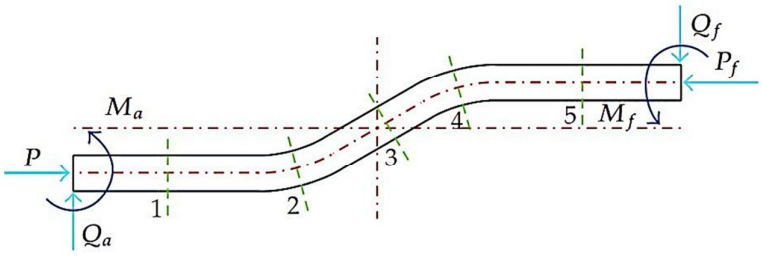

Fig3. Free-body diagram of the S-rail under the applied load P

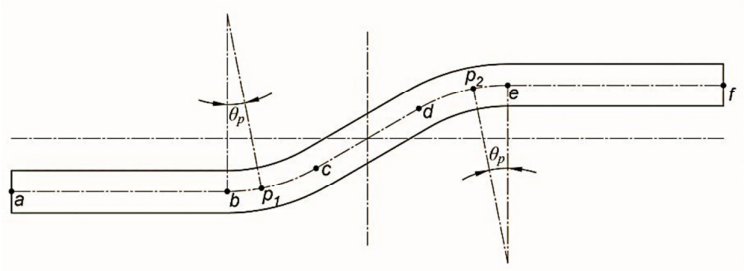

Fig4. Location of the critical points a, f, P_1 and P_2

Downloaded from www.iust.ac.ir at 20:04 IRST on Friday March 3rd 2017
[Downloaded from ijae.iust.ac.ir on 2026-09-12]
Created with nitroPDF professional
download the free trial online at nitropdf.com/professional

The axial force and bending moment at the point a can be obtained from [5]:

$$M_a = K_a * P \quad (1)$$

$$Q_a = J_a * P \quad (2)$$

Where:

$$K_a = \frac{gh' - g'h}{g'f - gf'}, \qquad J_a = \frac{fh' - f'h}{g'f - gf'} \quad (3)$$

$$f = \frac{l_{ab}^2}{2} + R(l_{ab}\theta + R(1-\cos\theta)) + ((l_{ab} + R\sin\theta)l_{cd} + \frac{l_{ab}^2}{2}\cos\theta) + R((l_{ab} + 2Rsin\,\theta + l_{cd}\cos\theta)\theta - R(1-\cos\theta)) + Ll_{ef}^3 - \frac{l_{ef}^2}{2} \quad (4)$$

$$g = \frac{l_{ab}^e}{3} + R(l_{ab}^2\theta + \frac{R^2}{2}(1-\cos 2\theta) + 2l_{ab}R(1-\cos\theta)) + ((l_{ab} + R\sin\theta)^2\, l_{cd} + \frac{l_{ef}^3}{3}\cos\theta + 2(l_{ab} + R\sin\theta)\cos\theta\frac{l_{cd}^2}{2}) + R((l_{ab} + 2R\sin\theta + l_{cd}\cos\theta)^2\,\theta + \frac{R^2}{2}(1-\cos 2\theta) - 2(l_{ab} + 2R\sin\theta + l_{cd}\cos\theta)R(1-\cos\theta)) + Ll_{cd}^3 - \frac{l_{cd}^2}{2} \quad (5)$$

$$h = R^2(l_{ab}(\theta - \sin\theta) + R(1-\cos\theta)) + R(1-\cos\theta)(l_{ab} + R\sin\theta)l_{cd} + \frac{l_{cd}^3}{6}\sin 2\theta + \frac{l_{cd}^2}{2}((\sin\theta(l_{ab} + R\sin\theta)) + R\cos\theta(1-\cos\theta)) + (R(1-2\cos\theta) + l_{cd}\sin\theta)((l_{ab} + 2R\sin\theta) + l_{cd}\cos\theta)R\theta - \frac{R^3}{4}(1-\cos 2\theta) + R^2(l_{ab} + 2R\sin\theta + l_{cd}\cos\theta)\sin\theta - R^2(R(1-2\cos\theta) + l_{cd}\sin\theta)(1-\cos\theta) + D\frac{l_{ef}^2}{2} \quad (6)$$

3. Position of neutral axis

Stress distribution across a fully plastic cross section is depicted in Figure 5.

For fully plastic sections, the axial force and bending moment are as following:

$$N_0 = \int YdA = YA \quad (14)$$

$$M_0 = \int YxdA = YQ \quad (15)$$

Where M_0 and N_0 are the fully plastic bending moment and fully plastic axial force, respectively. Also, Y is yield stress of constitutive material which is considered as 200MPa in the present work. Parameters A and Q in equations 14 and 15 are as following for square sections:

$$A = 4Wt \quad (16)$$

$$Q = \frac{3}{2}W^2t \quad (17)$$

where W is known as the web width and t is the wall thickness. Consequently, axial force and bending moment for a fully plastic section are equal to:

$$f' = l_{ab} + 2R\theta + l_{cd} + l_{ef} \quad (7)$$

$$g' = \frac{l_{ab}^2}{2} + R(l_{ab}\theta + R(1-\cos\theta)) + ((l_{ab} + \sin\theta)l_{cd} + \frac{l_{cd}^2}{2}\sin\theta) + ((l_{ab} + 2R\sin\theta + l_{cd}\cos\theta)\theta - (1-\cos\theta)) + \frac{l_{ef}^2}{2} \quad (8)$$

$$h' = R^2(\theta - \sin\theta) + R(1-\cos\theta)l_{cd} + \frac{l_{cd}^2}{2}\cos\theta + (R(1-2\cos\theta) + l_{cd}\sin\theta)\theta + R\sin\theta + Dl_{ef} \quad (9)$$

The axial force and bending moment at the point P_1 also can be obtained from [5]:

$$N_{p1} = L_pP \quad (10)$$

$$M_{p1} = K_pP \quad (11)$$

where:

$$L_p = \cos\theta_p + J_a * \sin\theta_p \quad (12)$$

$$K_p = K_a + R(1-\cos\theta_p) - J_a(l_{ab} + R\sin\theta_p) \quad (13)$$

At the equations 12 and 13, θ_p is an angle on the curved part which indicates location of the point p. When the external load P is applied, the S-rail deforms elastically until yield is reached in the extrme fibers on the most stressed sections. Assuming that the beam is made of elastic perfectly plastic material, increasing the external load, the plastic region in the cross section will be increased. In the limit, the whole section becomes plastic and then P =f_{max} . The load f_{max} is the collapse load which is also called peak crushing force.

$$M_0 = \frac{3}{2}YW^2t \quad (18)$$

$$N_0 = 4YWt \quad (19)$$

Because the section is under the axial force and bending moment simultaneously, neutral axis is not located in the center of section. Whereas the cross section is considered as squared tube, there are several different cases for neutral axis as following:

Case a: Neutral axis is positioned between center-line of the cross-section and inner surface of the web.

Case b: Neutral axis is in the web.

Case c: Neutral axis is outside of the cross-section.

Such three different case are shown in Figure 6.

According to the Figure 6, for each cases the following equations can be considered:

Case .a: $m = 1 - {}^4/_3\, n^2$ (20)

Case.b: $m = \frac{4}{3}(1-n)$ (21)

Case c: $m = 0 \quad n = \pm 1$ (22)

Created with nitroPDF professional
download the free trial online at nitropdf.com/professional
Downloaded from www.iust.ac.ir at 20:04 IRST on Friday March 3rd 2017
[Downloaded from ijae.iust.ac.ir on 2026-09-12]

where $m = \frac{M}{M_0}$ and $n = \frac{N}{N_0}$. In Figure 7, diagram of m-n is depicted and the cases a, b, c has been shown.

4 Effects of geometric parameters on the position of neutral axis

Due to geometrical dimensions, web width (w), wall thickness (t), curved angle (θ) and radius of curvature (R), one of the previous mentioned cases will be occurred at the critical points a and p (see Figure 4). Therefor by referring to geometrical parameters, position of neutral axis of the tube should be determined and then the peak crushing force can be calculated.

As it has been mentioned, with applying axial load on the S-rail, it deforms elastically and therefore by considering equations 1,2,10 and 11 bending to axial load ratio at the points a and P1 are as following:

$$\frac{M_a}{N_a} = K_a \quad (23)$$

$$\frac{M_p}{N_p} = \frac{K_p}{L_p} \quad (24)$$

Cross sectional axial and bending loads are increased by increasing the external load. Therefore, axial and bending loads at the critical sections (a and P1) will be increased by increasing the external load until the stress value at the outer fiber of cross section reach to yield. In this paper, it is assumed that the bending to moment ratio is remained constant after onset of plastic yielding at the outer fiber. So the relations between bending and moment at the critical cross sections a and P1 can be obtained from:

$$m_a = K_a \frac{N_0}{M_0} n_a \quad (25)$$

$$m_p = \frac{K_p}{L_p} \frac{N_0}{M_0} n_p \quad (26)$$

Equations 25 and 26 will be called as load line equations in the following sections. Related Load lines to each section could be depicted in the similar surface of m-n diagram. When one load line cross each case diagram could guide to find the exact position of neutral axis. Following, the effect of parameters including radius of curvature (R), curved angle (θ) and web width (w) in neutral axis are studied. Effect of geometrical parameters on the position of neutral axis at point a is shown in Figure 8 which the value of geometrical dimensions is basis on R=550 mm, $\theta = 25^\circ$, t=2 mm and W=50.

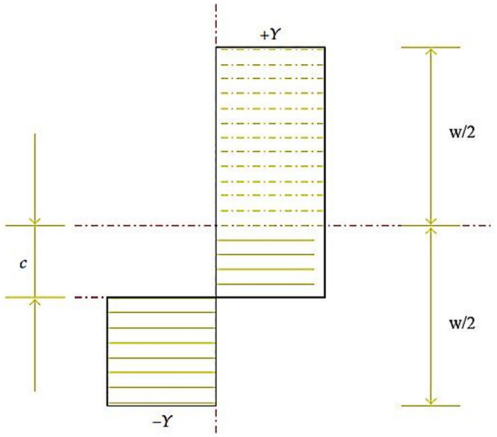

Fig5. stress distribution in the section of a fully plastic [6]

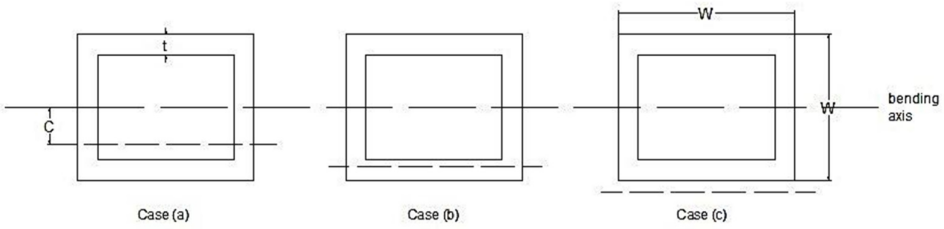

Fig6. position of the neutral axis

Created with nitroPDF professional
download the free trial online at nitropdf.com/professional
Downloaded from www.iust.ac.ir at 20:04 IRST on Friday March 3rd 2017
[Downloaded from ijae.iust.ac.ir on 2026-09-12]

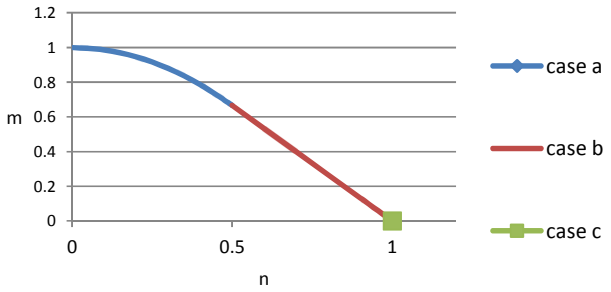

Fig7. Diagram of different cases of natural axis

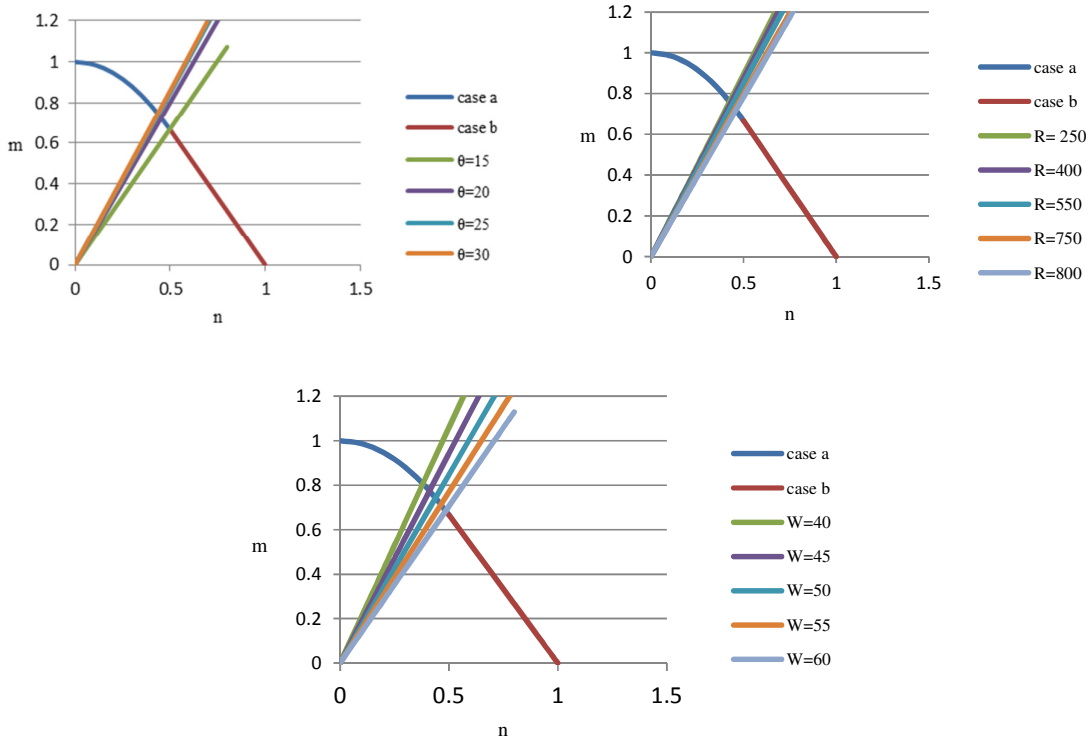

Fig8. Effect of geometrical design parameters on the position of neutral axis at the critical point a

Figure 9 shows the similar diagrams of the figure 8 for the critical point P.

In Figure 10, effects of each geometrical parameters on the slope of load line which is effective to determine the position of neutral axis is shown.

Figures 8 to 10 clearly show that the radius of curvature has the opposite relationship with slope of load line and slope of this diagram is going down by increasing the radius. This decreasing of slope of load line which is caused by increasing of radius, will be speeded up at point a. In the other hand with increasing the curved angle (θ), slope of load line is going up too at points a and P1. The slope of load line also will be decreased by increasing web width at points a and P1.

The values of geometrical parameters which cause each cases of a and b at the points a and P for the basic geometry (t=2 mm, w=50 mm, θ = 25, R=550 mm) are presented in table 1.

Created with nitroPDF professional
download the free trial online at nitropdf.com/professional
Downloaded from www.iust.ac.ir at 20:04 IRST on Friday March 3rd 2017
[Downloaded from ijae.iust.ac.ir on 2026-09-12]

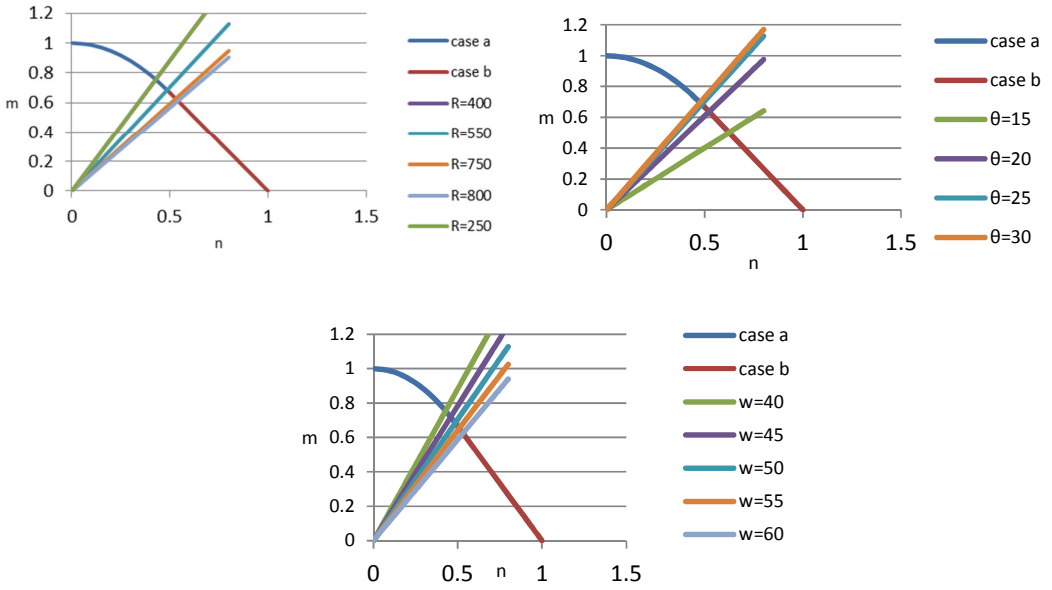

Fig9. Effect of geometrical design parameters on the position of neutral axis at the critical point p.

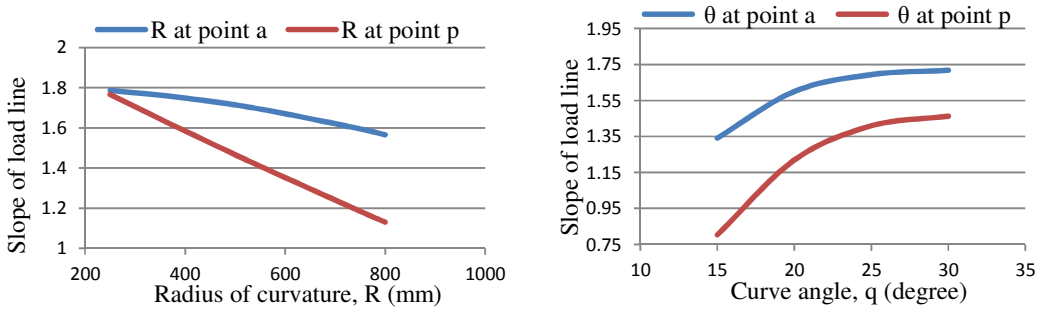

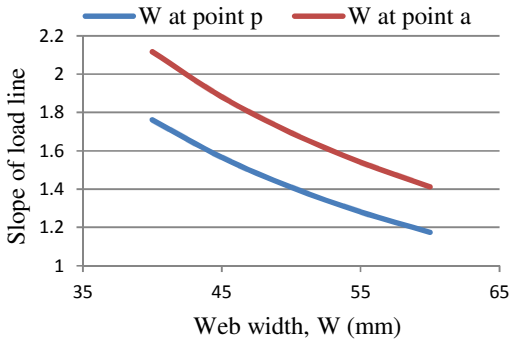

Fig10. Effect of geometrical parameters on the slope of load line in the critical points a and p

Created with nitroPDF professional
download the free trial online at nitropdf.com/professional
Downloaded from www.iust.ac.ir at 20:04 IRST on Friday March 3rd 2017
[Downloaded from ijae.iust.ac.ir on 2026-09-12]

Downloaded from www.iust.ac.ir at 20:04 IRST on Friday March 3rd 2017

[Downloaded from ijae.iust.ac.ir on 2026-09-12]

Table 1- Values of geometrical parameters which cause each cases of a and b at the points a and P for the basic geometry of t=2 mm, w=50 mm, $\boldsymbol{\theta = 25}$ and R=550 mm

R	θ	W	T	Case	
R<1000 mm	25	50 mm	2 mm	Case a	Point a
550	θ>14	50 mm	2 mm	Case a	
550	25	W<65 mm	2 mm	Case a	
R>1000 mm	25	50 mm	2 mm	Case b	
550	θ<14	50 mm	2 mm	Case b	
550	25	W>65 mm	2 mm	Case b	
R<650 mm	25	50 mm	2 mm	Case a	Point p
550	θ>20	50 mm	2 mm	Case a	
550	25	W<55 mm	2 mm	Case a	
R>650 mm	25	50 mm	2 mm	Case b	
550	θ<20	50 mm	2 mm	Case b	
550	25	W>55 mm	2 mm	Case b	

5. Extraction of peak crushing force

Based on determined position of neutral axis at points a and P1, calculation of peak crushing force is already possible. The equation of axial load and bending moment along cross section could be written as below:

$$M = \int \sigma x dA = Ytb^2 + 2Yt((\frac{W^2}{2}) - c^2) \quad (27)$$

$$N = \int \sigma dA = 4Ytc \quad (28)$$

where Y is known as the yield stress of the material and c is location of neutral axis which is shown in figure 5. Considering section a as critical section and also assuming occurrence of case a at this section, below equation will be derived as following by substituting equation 1 in equation 20 and considering Na = P:

$$\left(\frac{4}{3N_0^2}\right)P^2 + \left(\frac{K_a}{M_0}\right)P - 1 = 0 \quad (29)$$

From solving above equation, $F_{max,1}$ can be derived as following:

$$F_{max,1} = \frac{\left(\frac{K_a}{M_0}\right) + \sqrt{\left(\frac{K_a}{M_0}\right)^2 + \left(\frac{4}{3N_0^2}\right)}}{2\left(\frac{4}{3N_0^2}\right)} \quad (30)$$

Also considering section a as critical section and assuming occurrence of case b at this section, below equation will be derived as following by substituting equation 1 in equation 21:

$$\left(\frac{K_a}{M_0}\right)P + \left(\frac{4}{3N_0}\right)P = \frac{4}{3} \quad (31)$$

From solving above equation, $F_{max,1}$ will be derived as following:

$$F_{\max,1} = \left(\frac{4/3}{\left(\frac{K_a}{M_0}\right) + \left(\frac{4}{3N_0}\right)}\right) \quad (32)$$

Considering section P1 as critical section and assuming occurrence of case a at this section, below equation will be derived as following by substituting equation 10 and 11 in equation 20:

$$\left(\frac{4l_p^2}{3N_0^2}\right)P^2 + \left(\frac{K_p}{M_0}\right)p - 1 = 0 \quad (33)$$

From solving above equation, $F_{max,2}$ will be derived as following:

$$F_{max,2} = \frac{\left(\frac{K_p}{M_0}\right) + \sqrt{\left(\frac{K_p}{M_0}\right)^2 + \left(\frac{4l_p^2}{3N_0^2}\right)}}{2\left(\frac{4l_p^2}{3N_0^2}\right)} \quad (34)$$

Also considering section P1 as critical section and assuming occurrence of case b at this section, below equation will be derived as following by substituting equation 10 and 11 in equation 20:

$$\left(\frac{K_p}{M_0}\right)F + \left(\frac{4l_p}{3N_0}\right) = \frac{4}{3} \quad (35)$$

From solving above equation, $F_{max,2}$ will be derived as following:

Created with nitroPDF professional
download the free trial online at nitropdf.com/professional

$$F_{\max,2} = \left(\frac{4/3}{\left(\frac{K_p}{M_0}\right)+\left(\frac{4l_p}{3N_0}\right)} \right) \quad (36)$$

Position of neutral axis could be determined according to equations represented in section 3 after determining geometrical dimensions of S-rail. The values of $F_{max,1}$ and $F_{max,2}$ could be calculated after finding the position of neutral axis .The minimum value between Fmax,1 and Fmax,2 will be selected as peak crushing force of the S-rail, because before the value of P reaches to maximum value of Fmax , plastic collapse will be occurred in minimum value of Fmax .

$$F_{max} = \min\{F_{max,1}, F_{max,2}\} \quad (37)$$

6. Numerical simulation

Explicit finite element method has proven valuable in solving quasi-static problem. However, it should be noted that the explicit solution method is developed to model the events in which inertia plays a dominant role in the solution such as high speed dynamic impact problems. Moreover, the loading rate applied in actual quasi-static experiments, 5 mm/min is too slow which increases the time step too much. Therefore, to perform an accurate, low-cost and reliable quasi-static analysis, the inertia effects and the time step must be reduced, simultaneously. There are two special approaches which could be employed in combination to perform accurate and economic quasi static analyses using explicit procedure.

3.1. Mass scaling

The minimum stable time increment in the explicit dynamic analysis can be expressed as

$$\Delta t = L^e \sqrt{\frac{\rho}{E}} \quad (38)$$

Where Le is the element length characteristic, E is the young's modulus, and ρ is the material density. According to the Eq. (29), artificially scaling up the material density by factor of f^2 increases the stable time increment by factor of f. Therefore total time step will be decreased because fewer increments required to perform the same analysis. Scaling uo the mass, however, increases the inertia effects. Therefore, to ensure the quasi-static process, the loading rate should be kept very low. Another mass scaling method is the scaling down the mass of the material so that the inertial forces trial forces will be minimized. When the mass is scaling down, the stable time increments are increased and the time step of analysis will also be increased. Therefore, to reduce the time step, the loading rate must be accelerated.

3.2. Smooth load curve

Sudden movements cause stress waves which can induce noisy or inaccurate solution. Therefore, it is needed to apply loading as smooth as possible. A typical smooth loading curve is shown in Fig. 11. It is clear from this figure, that initial velocity and initial slope of curve which is equal to initial acceleration are zero. This ensure that loading takes place gradually and unnecessary dynamic effects will be avoided.

Several investigators have employed explicit procedure for quasi-static analysis. Meguid et al. [7] for the used LSDYNA for the quasi-static simulation of foam-filled columns. They employed mass scaling of 10 to reduce the required solution time. They showed that the total kinetic energy and the crushing force-displacement response did not change with scaling. Aktay et al. [8] also used PAMCRASH for the quasi-static simulation for extruded poly styrene from filled thin-walled aluminum where mass scaling of 1/1000 and applied velocity V=2 m/s have been considered. Nagel et al. [9] employed ABAQUS/Explicit for the quasi-static simulation of tapered thin-walled tubes under oblique loading. The loading rate was controlled using the AMPLITUDE option and SMOOTH STEP sub-option in ABAQUS/Explicit to ensure an accurate and efficient quasi-static analysis.

After a quasi-static analysis two type of tests are used for evaluating the results of simulation. First, if a simulation is quasi-static, the velocity of the material is very small and so that internal forces are negligible. Therefore, in this situation, internal energy is nearly equal to the work applied by the external forces while the kinetic energy is small and should not exceed a small fraction of internal energy. Secondly, the load displacement response must be independent from mass scaling and loading rates.

Load and boundary conditions consider in the present finite element simulation of the s-rail are shown in Figure 2. In this finite element analysis, the flat plate which is applying the load is modeled as a rigid surface and all degrees of its freedom are bounded except move in the direction of the applied load. The other end of S-rail is completely attached to a rigid surface by Tie bonded. The compressive load is applied to the S-rail by applying a constant velocity to the loaded end. The smooth amplitude is also used for applying the velocity.

Downloaded from www.iust.ac.ir at 20:04 IRST on Friday March 3rd 2017
[Downloaded from ijae.iust.ac.ir on 2026-09-12]
Created with nitroPDF professional
download the free trial online at nitropdf.com/professional

The shape of deformation of the S-rail with geometries of R=550 mm , q=25 , W=50 mm and t=2 mm are shown as examples in Figure 12. These shapes of deformation are at the end displacement reached to the values of 150, 250 and 400 mm

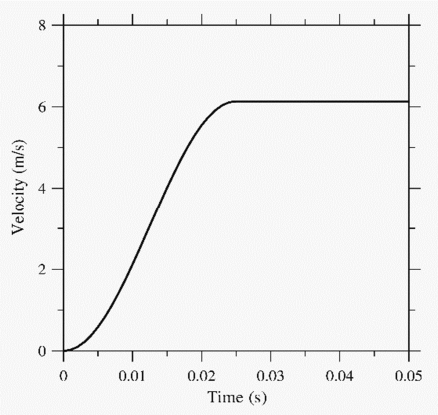

Fig11. Typical smooth loading curve

Displacement=150 mm Displacement= 250 mm Displacement=400 mm

Fig12. shape of deformation of the S-rail with geometries of R=550 mm , q=25 , W=50 mm and t=2 mm at end displacement of 150, 250 and 400 mm.

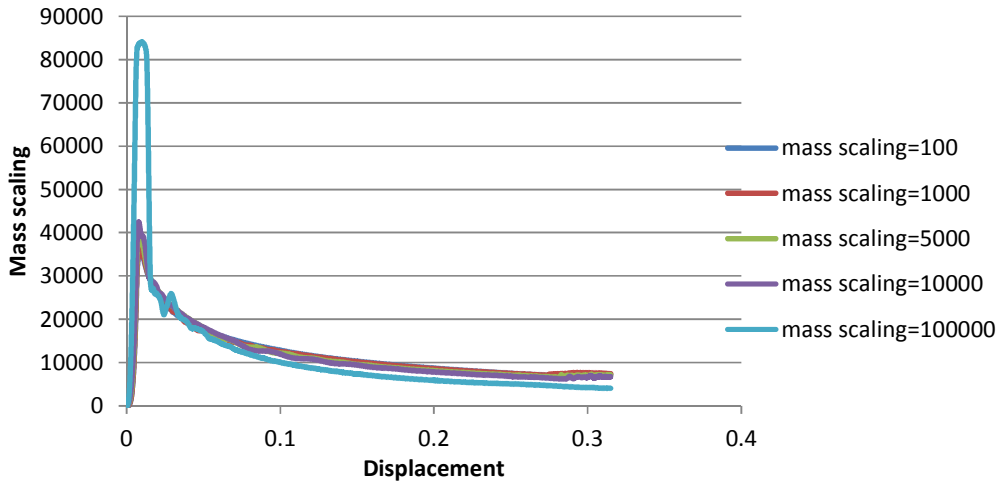

Fig13. Comparison of load-displacement diagram carried out with different values of mass scaling

Created with nitroPDF professional
download the free trial online at nitropdf.com/professional
Downloaded from www.iust.ac.ir at 20:04 IRST on Friday March 3rd 2017
[Downloaded from ijae.iust.ac.ir on 2026-09-12]

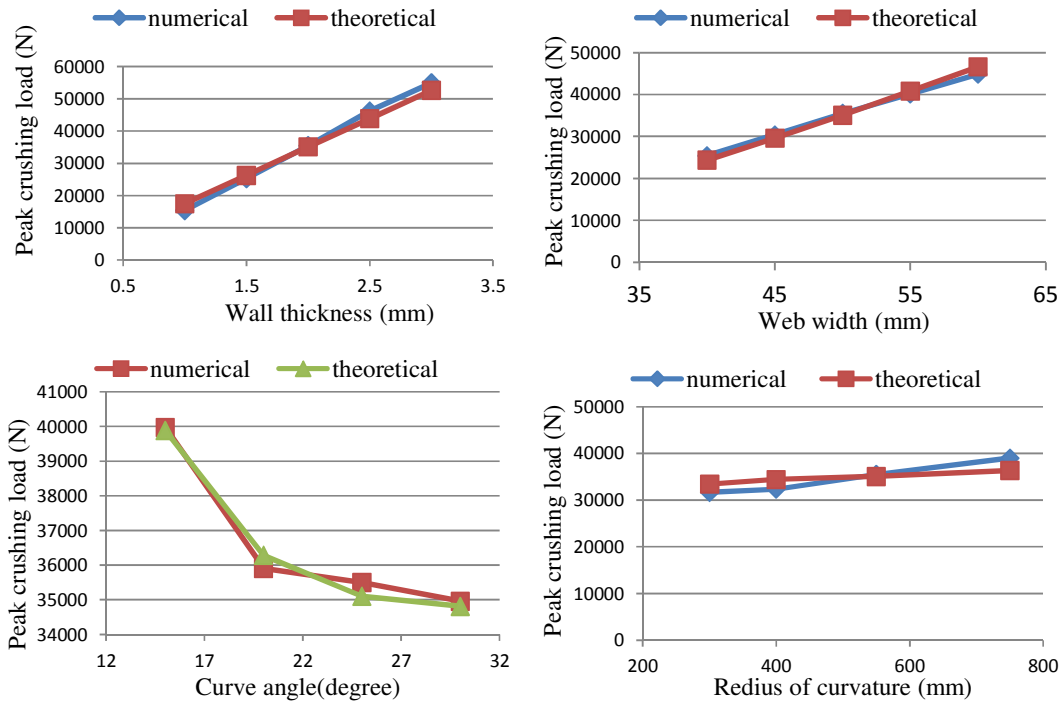

Fig14. Comparison between theoretical and numerical results respective to different values of geometrical design variables

Table 2.comparison between numerical and theoretical results

Raws	W (mm)	t (mm)	R (mm)	θ (degree)	F_{max} (N)		
					Numerical	Theoretical	Error
1	50	1	550	25	15414	17550.9	12
2	50	1.5	550	25	25290	26326	4
3	50	2	550	25	35499	35101.9	1.13-
4	50	2.5	550	25	46275	43877.4	5.46-
5	50	3	550	25	54985	52652	4.43
6	40	2	550	25	25418	24377	4.27-
7	45	2	550	25	30391	26619	14.1-
8	50	2	550	25	35499	35101	1.13-
9	55	2	550	25	40152	40799	1.6
10	60	2	550	25	44894	46619	3.7
11	50	2	550	15	39978	39887	0.23-
12	50	2	550	20	35906	36283	0.1
13	50	2	550	25	35499	35101	1.13-
14	50	2	550	30	34959	34810	0.4-
15	50	2	250	25	31672	33456	5.3
16	50	2	400	25	32352	34441	6
17	50	2	550	25	35499	35101	1.13-
18	50	2	750	25	39014	36347	7.3-

Downloaded from www.iust.ac.ir at 20:04 IRST on Friday March 3rd 2017
[Downloaded from ijae.iust.ac.ir on 2026-09-12]
Created with nitroPDF professional
download the free trial online at nitropdf.com/professional

Downloaded from www.iust.ac.ir at 20:04 IRST on Friday March 3rd 2017

[Downloaded from ijae.iust.ac.ir on 2026-09-12]

Load-displacement diagram of the S-rail shown in figure 12 is depicted in figure 13. For selecting prior value of mass scaling, five different values of mass scaling are considered and compared in the figure 13.

Following, obtained results of peak crushing force from analytical and numerical models are compared. These analyses are based on the geometrical values of $\theta = 25^{\circ}$, t=2 mm, W=50 mm and R=550 mm. Comparison between theoretical and numerical results respective to different values of web width (W), wall thicknesses (t), radius of curvature (R) and curve angle (θ) are shown in the Figure 14.

The values of geometrical design parameters and obtained results for peak crushing force from numerical and analytical analyses correspond to the Figure 22 to 25 are presented in table 2.

Conclusion

In this paper, at the first step, peak crushing force is derived based on the position of neutral axis of beam and also the effect of position of neutral axis respective to peak crushing force is analyzed. At the next step, quasi-static analysis of the s-rail is performed using commercial software ABAQUS/Explicit and peak crushing force is determined.

At the last step, comparison of numerical and analytical results is performed. Such comparison shows good agreement between the obtained results. Consequently useful equations are derived which can be employed for calculating of peak crushing force of s-rail that can be used for design of such structures.

REFERENCES

[1]. Ni, C. M., "Impact Response of Curved Box Beam Columns with Large Global and Local Deformations.Proceedings of the 14thStructures," Structural Dynamics, and Materials Conference, King of Prussia, PA, U.S.A. AIAA pp. 73-401 (1976).

[2]. Kim, H-S. and Wierzbicki, T., "Effect of the Cross-Sectional Shape on Crash Behavior of a 3-D Space Frame," Impact and Crashworthiness Laboratory Report No. 34, MIT (2000).

[3]. Kim, H. S. and Wierzbicki, T., "Closed-Form Solution for Crushing Response of Three-Dimensional Thin-Walled S Frames with Rectangular Cross-Sections," International Journal of Impact Engineering, 30, pp. 87□112 (2004).

[4]. Zheng, L. and Wierzbicki, T., "Quasi-Static Crushing of S-Shaped Aluminum Front Rail, "International Journal of Crashworthiness, 9, pp. 155-173 (2004).

[5]. A.khalkhali, A. Darvizeh, A. masoumi, N.Nariman-zadeh and A. shiri, Robust Design of S-Shaped Box Beam Subjected to Compressive Load, journal Mathematical Problem in Engireneering 627501m (2010)

[6]. Heung-soo kim , Tomasz wierzibicki, Crash behavior of thin-walled prismatic column under combined bending and compression. 79 (2001) 1417_1432

[7]. Meguid, S. A., Stranart, J. C. and Heyerman, J .,"On the Layered Micromechanical Three-Dimensional Finite Element Modeling of Foam-Filled Columns," International Journal of Finite Elements in Analysis and Design, 40, pp.1035・1057 (2004).

[8]. Aktay, L., Toksoy, A. K. and Guden, M., "Quasi-Static Axial Crushing of Extruded Polystyrene Foam-filled Thin-Walled Aluminum Tubes:Experimental and Numerical Analysis," International Journal of Materials and Design, 27, pp. 556・565 (2006).

[9]. Nagel, G. M. and Thambiratnam, D. P., "Dynamic Simulation and Energy Absorption of Tapered Thin-Walled Tubes Under Oblique Impact Loading," International Journal of Impact Engineering, 32, pp. 1595・1620 (2006).

Created with nitroPDF professional
download the free trial online at nitropdf.com/professional